Role of atomic structure on grain boundary-defect interactions in Cu

Xian-Ming Bai,[1] Louis J. Vernon,[2] Richard G. Hoagland,[2] Arthur F. Voter,[3] Michael Nastasi,[4] and Blas Pedro Uberuaga[2]
[1]*Center for Advanced Modeling and Simulation, Idaho National Laboratory, Idaho Falls, Idaho 83415, USA*
[2]*Materials Science and Technology Division, Los Alamos National Laboratory, Los Alamos, New Mexico 87545, USA*
[3]*Theoretical Division, Los Alamos National Laboratory, Los Alamos, New Mexico 87545, USA*
[4]*Materials Physics and Applications Division, Los Alamos National Laboratory, Los Alamos, New Mexico 87545, USA*
(Received 23 January 2012; revised manuscript received 9 May 2012; published 4 June 2012)

We investigate the role that the atomic structure of grain boundaries in Cu has in the interaction with point defects produced during irradiation. We focus on three aspects of boundary-defect interaction: how defects interact with pristine boundaries, how boundaries modify defect production during collision cascades, and how defects interact with damaged boundaries. We find that there are generic features common to most boundaries, including biased absorption of interstitials over vacancies during collision cascades and strong interactions with vacancies for interstitial-loaded boundaries. However, we find that the magnitude of these behaviors depends strongly on the atomic structure of the boundary. In particular, the biased absorption is much stronger for a high-angle twist boundary and smallest for a more general twist-asymmetric tilt boundary. Further, the strength of boundary-defect interactions is also sensitive to the boundary structure. We conclude that the sink strength of grain boundaries for interacting with point defects is not an intrinsic property of the boundary but rather depends on the irradiation conditions through the absorbed defect content at the boundary.

DOI: 10.1103/PhysRevB.85.214103 PACS number(s): 61.72.Mm, 61.72.J−, 66.30.Pa, 07.05.Tp

I. INTRODUCTION

Interfaces such as grain boundaries (GBs) play a critical role in numerous properties of materials, from mass transport[1,2] to electronic conductivity[3] to material strength.[4,5] In particular, radiation tolerance is very sensitive to the interfacial content of the material. Decades of work have demonstrated that GBs act as sinks for radiation-induced defects, creating defect denuded zones near the boundaries.[6–8] More recently, improved synthesis methods have led to materials that have an extraordinarily high density of interfaces. Irradiation studies have demonstrated that these materials, from nanocrystalline single-phase materials[9–12] to multilayer nanocomposites,[13] can have radiation tolerance far superior to large-grained counterparts, although under certain conditions, GBs have been shown to worsen radiation tolerance.[10,14]

The majority of the work on the role of GBs and interfaces on radiation tolerance have not distinguished the differences that might result from GB structure. While it has been demonstrated that different GBs do indeed influence phenomena such as segregation,[15,16] defect mobility,[15,17,18] and the thermodynamics of defects,[19–22] how the atomic structure of the GB modifies damage production and subsequent defect evolution during irradiation has received little attention. Pérez-Pérez and Smith showed that GBs absorb interstitials during collision cascades in Fe.[23] Samaras *et al.*[24] found that cascades interacting with GBs in Ni modify the damage produced significantly,[25] leading to enhanced production of stacking-fault tetrahedra, which they related to the dislocation structure of the GBs. Interestingly, such effects are not observed in simulations of SiC.[11] In our previous work, we showed how, during collision cascades, a symmetric-tilt GB in Cu preferentially absorbs interstitials, leaving an excess concentration of vacancies in the bulk region of the material.[26] We then described an atomic-scale mechanism in which those "loaded" interstitials interacted with the residual vacancies over relatively long distances and short time scales. Together with accelerated conventional diffusion of vacancies to GBs, this mechanism leads to enhanced defect recombination in nanocrystalline materials. Here, we examine five GBs in Cu with different atomic structures and determine how that structure influences radiation damage, emphasizing both the generality of the observed behavior as well as differences that are attributed to GB atomic structure. We conclude that while there is behavior generic to most of these GBs, there are also significant differences that must be accounted for to accurately predict the evolution of the material under irradiation.

II. METHODOLOGY

We examine the role that the atomic structure of grain boundaries in Cu has in influencing the thermodynamic and kinetic properties of radiation-induced defects using molecular statics, molecular dynamics (MD), and saddle-point searching methods. In particular, we are interested in how defects interact with both pristine GBs and GBs damaged by radiation. We have examined the properties of five GBs: $\Sigma 3$ coherent twin, $\Sigma 5$ twist, $\Sigma 11$ symmetric tilt, $\Sigma 11$ asymmetric tilt, and $\Sigma 45$ asymmetric tilt/twist (this shorthand notation, used here for simplicity, does not fully characterize a given GB; full orientations for the GBs studied here are given in Table I). The Σ number is the ratio of the cell volume of the coincidence site lattice to the cell volume of the elementary unit cell of the generating lattice. These GBs are representative of the complex nature of boundaries in materials, from the $\Sigma 3$ twin, an extremely low-energy GB, to the $\Sigma 45$, a very high-energy GB with mixed tilt, twist, and asymmetric character, representative of so-called "general" GBs. To determine how these GBs influence radiation damage, we have focused on three aspects of boundary-defect interaction that are crucial for understanding radiation damage evolution: (a) the interaction of point defects with the pristine GB, (b) changes in the production of radiation-induced defects by the GB, and (c) the subsequent interaction of defects with the damaged GB.

TABLE I. Orientation relationships and applied rotations for the boundaries discussed in this paper. For the three pure tilt GBs, the z axis is the rotation axis and y is the direction normal to the GB plane in each grain. For the $\Sigma 5$ twist GB, the y axis is both the rotation axis and the direction normal to the GB plane. For the $\Sigma 45$ GB, the y axis is the direction normal to the GB plane in each grain, the tilt rotation axis is along z, and the twist rotation axis is along y.

	Upper grain			Lower grain		
Boundary	x	y	z	x	y	z
$\Sigma 3$ twin	$[12\bar{1}]$	$[11\bar{1}]$	[101]	$[12\bar{1}]$	$[\bar{1}11]$	[101]
$\Sigma 5$ twist	$[30\bar{1}]$	[010]	[103]	[301]	[010]	$[\bar{1}03]$
Symmetric $\Sigma 11$ tilt	$[32\bar{3}]$	$[\bar{1}31]$	[101]	$[32\bar{3}]$	$[13\bar{1}]$	[101]
Asymmetric $\Sigma 11$ tilt	$[54\bar{5}]$	$[\bar{2}52]$	[101]	$[18\bar{1}]$	$[\bar{4}14]$	[101]
$\Sigma 45$	[210]	[001]	$[1\bar{2}0]$	$[01\bar{2}]$	[221]	$[54\bar{2}]$

The grain boundary structures were found by constructing an initial bicrystal with the orientation relationships and applied rotations described in Table I. These specify the five macroscopic degrees of freedom of the GB. The two microscopic degrees of freedom are determined by mapping the gamma surface and finding the lowest-energy structure. The shorthand used in this paper for the various boundaries specifically refers to this lowest-energy structure. The atomic structure of each of the boundaries found in this way is shown in Fig. 1 and their energies are listed in Table II. The Mishin *et al.* EAM potential[27] is used for all calculations in this work. The simulation cells used are similar to those described in Ref. 26 containing a moving region sandwiched between two rigid regions. The number of moving atoms and total number of atoms for mapping the gamma surface ranged between 1485–2460 and 2295–4050, respectively.

We note that in some cases, particularly the asymmetric $\Sigma 11$ boundary, the structure of the gamma surface is slightly different depending on the system size. For example, while the calculated gamma surfaces for the asymmetric $\Sigma 11$ GB for two different system sizes (one with 2950 atoms and dimensions in the GB plane of 29.4 Å × 12.8 Å, and a second with 4020 atoms and dimensions of 29.4 Å × 25.6 Å) are overall similar, there are quantitive differences. In the calculations reported here, we used the lowest-energy structure found on the 2950-atom gamma surface.

MD is then used to study cascade-induced damage near the GBs at 300 K, in a manner similar to that in Ref. 26. The total number of atoms ranged from 144 960 to 163 620, while the number of moving atoms ranged from 119 520 and 134 460. An atom is chosen as the primary knock-on atom (PKA) with 4 keV of kinetic energy, directed perpendicularly towards the GB. The final damaged structure is compared to the undamaged structure with the reference lattice site method to characterize defects, using a cutoff distance of 1.0 Å. Only the defects remaining in the bulk region are counted as surviving defects, and two defects belong to the same cluster if their separation is less than 2.7 Å. In each cluster, only the net number of defects is counted. At each PKA distance, 10 (for $\Sigma 5$) or 15 (for all other GBs) cascade simulations are performed. Results are compared to cascades in a single crystal with the same PKA direction relative to the crystallographic orientation as in the cascade simulations for each GB.

As we discuss both below and in Ref. 26, the primary conclusion from the cascade simulations is that interstitials are preferentially absorbed by the GB. Temperature-accelerated dynamics simulations reported in Ref. 26 found that those interstitials could interact with residual vacancies in the bulk, annihilating them with relatively small barriers and over long distances. To investigate these "interstitial emission" processes systematically, we load GBs with 10 interstitials using MD. To reach a loading of 10, interstitials are placed near the GB plane and annealed. The formation energies of vacancies near the interstitial-loaded GBs are then calculated for each site near the interstitial-loaded GBs. This is compared to vacancy formation energies near the pristine GB structures. In the case of the pristine GBs, we also calculated the interstitial formation energies by first identifying interstitial sites using the method of Jiang *et al.*[28] and then minimizing the energy for an interstitial at that position.

Finally, we examine the recombination barriers for vacancies and interstitials near interstitial-loaded GBs. We first identify sites that have negative vacancy formation energies, which is a signature of spontaneous recombination with interstitials at the boundary. Having ascertained and excluded the vacancy sites corresponding to spontaneous recombination, the remaining sites were examined for finite-barrier recombination processes. For every vacancy location, hundreds of transition searches were performed using the

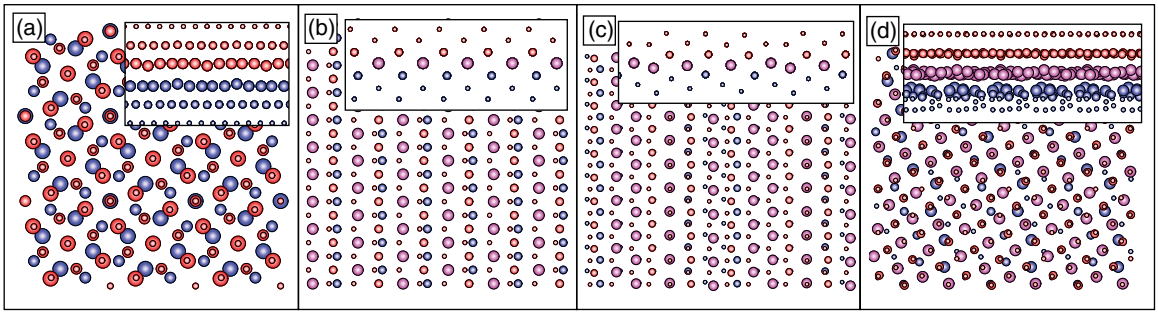

FIG. 1. (Color online) Structure of the four grain boundaries considered here: (a) $\Sigma 5$ twist, (b) symmetric $\Sigma 11$ tilt, (c) asymmetric $\Sigma 11$ tilt, and (d) $\Sigma 45$ asymmetric tilt plus twist. In each figure, the structure is shown down the grain boundary normal, while the insets show the structure perpendicular to the grain boundary normal. The atoms are colored and sized by position: red atoms are in the upper grain, blue atoms are in the lower grain, purple atoms are on the boundary plane, and the size of atoms is larger as their distance to the grain boundary plane decreases.

TABLE II. Summary of various GB properties determined in this study. The energy of the Σ3 twin boundary is 0.02 J/m^2. This GB has no discernible interaction with point defects, so it is not included in the table. The interaction strength is defined as the difference in energy of the defect in the bulk versus the lowest-energy site at the grain boundary. The interaction width is defined as the summed distance on both sides of the GB to which defect energies differ by more than 10% from their bulk values for the pristine GBs. d_{0K} is the width, measured relative to the number of sites with negative formation energy, of the recombination zone for sites exhibiting spontaneous recombination, d_{finite} is the width of the recombination zone when sites with finite-barrier processes are also included, N_{0K} is the number of sites with spontaneous recombination, and N_{finite} is the number of sites with finite-barrier recombination processes, all measured for the interstitial-loaded GBs.

		Pristine boundary properties							
		Interaction strength (eV)		Interaction width (nm)		Loaded boundary properties			
Boundary	Energy (J/m^2)	Vacancy	Interstitial	Vacancy	Interstitial	d_{0K} (nm)	d_{finite} (nm)	N_{0K}	N_{finite}
Σ5 twist	0.73	0.5	2.4	0.22	1.50	0.8	1.5	135	194
Symmetric Σ11 tilt	0.31	0.2	1.6	0.20	0.92	1.0	1.9	164	295
Asymmetric Σ11 tilt	0.66	0.7	2.4	0.8	3.02	1.1	1.6	74	292
Σ45	0.89	1.1	3.0	0.7	2.19	0.9	1.3	76	170

relaxation and translation method[29] in order to determine the lowest barrier recombination process available. Once several hundred searches had been performed finding no lower-energy processes, the calculation was concluded.

Determining the barriers for recombination events requires a definition of when an event leads to recombination, as opposed to, for example, a vacancy hop. For most boundaries, it is safe to assume that, after an event involving a vacancy, a vacancy formation energy less than 0 eV corresponds to such an annihilation via an emission event. However, Fig. 2 demonstrates that this is not a safe criterion for all four boundaries. Examining the formation energy density, or the number of events of any type with a given final (after the event) formation energy, for the symmetric tilt Σ11 GB reveals a clearly defined gap at 0 eV, and visual inspection of the events shows that vacancy formation energies above 0 eV correspond to vacancies that are stable, while those below 0 eV correspond to interstitial-vacancy annihilation.

For the Σ45 boundary, however, the situation is not as clear, with the 0-eV threshold lying within a cluster of vacancy formation energies. Further, vacancy annihilation events are seen close to, but higher than, the 0-eV threshold; that is, we observe recombination events that correspond to positive (although only slightly, less than 0.03 eV) vacancy formation energies. As such, the nearest minimum above 0 eV in vacancy formation energy density was taken to be the threshold for defining if the event led to recombination. This was only an issue for the Σ45 boundary and is possibly due to system-size effects in the determination of the vacancy formation energy.

III. RESULTS

A. Defect interaction with the pristine boundaries

Figure 3 shows the formation energy of interstitials and vacancies near each of the four nontwin GB structures considered as a function of the initial distance of the defect from the boundary plane. The data for the vacancy formation energy near the pristine Σ11 GBs, both symmetric and asymmetric, were originally presented in Ref. 26. Except in the case of the Σ3 twin, which we will discuss separately below, there are a number of features common to all of these boundaries, although there are also significant differences. First, for the nontwin GBs, interstitials interact with the GB much more strongly than vacancies do. This is reflected in both the changes in formation energy as the defects are placed nearer the boundary plane as well as the width of the region over which the defects experience significant changes in energy. If we consider a GB as being a strong sink when defect formation energies are reduced by over 40%, all of these boundaries are strong sinks for interstitials, but only the asymmetric Σ11 and Σ45 GBs are strong sinks for vacancies.

As mentioned, the Σ3 twin is a special case. This GB has very weak interaction with vacancies (the reduction of the vacancy formation energy is less than 0.8%) and no discernible interaction with interstitials. This result indicates that the coherent twin GB is not a sink for defects, consistent with the results of Demkowicz *et al.*[30] Interestingly, however, they found that this GB still mediated enhanced defect recombination, in spite of the very weak interaction with defects.

While there are features generic to the four nontwin GBs, the details depend on the GB structure. Considering the distance at which the defects directly interact with the GB, as indicated by the width of the highlighted regions in Fig. 3 and defined as the distance over which sites exist where the defect formation energy is at least 10% lower than in the bulk, there is great variability between the four structures, with the symmetric Σ11 having the smallest interaction zone and the asymmetric Σ11 having the greatest. However, the strength of interaction shows a different trend. The symmetric Σ11 also has the weakest strength of interaction with both interstitials and vacancies, while the Σ45 GB has the strongest. The other two GBs lie in-between. The Σ45 GB is nearly a perfect sink for both interstitials and vacancies; the lowest formation energy for each at this GB is only 0.3 and 0.2 eV, respectively, significantly lower than the respective 3.25 and 1.27 eV in the bulk. These results are summarized in Table II, where the interaction strength is defined as the difference in energy between the defect in the bulk and the defect at the lowest energy site at the GB.

Some of these differences are a clear consequence of the atomic structure of the GB. For example, the asymmetric Σ11 GB is characterized by Schockley partial dislocations, which extend out of the GB into the upper grain. This results in

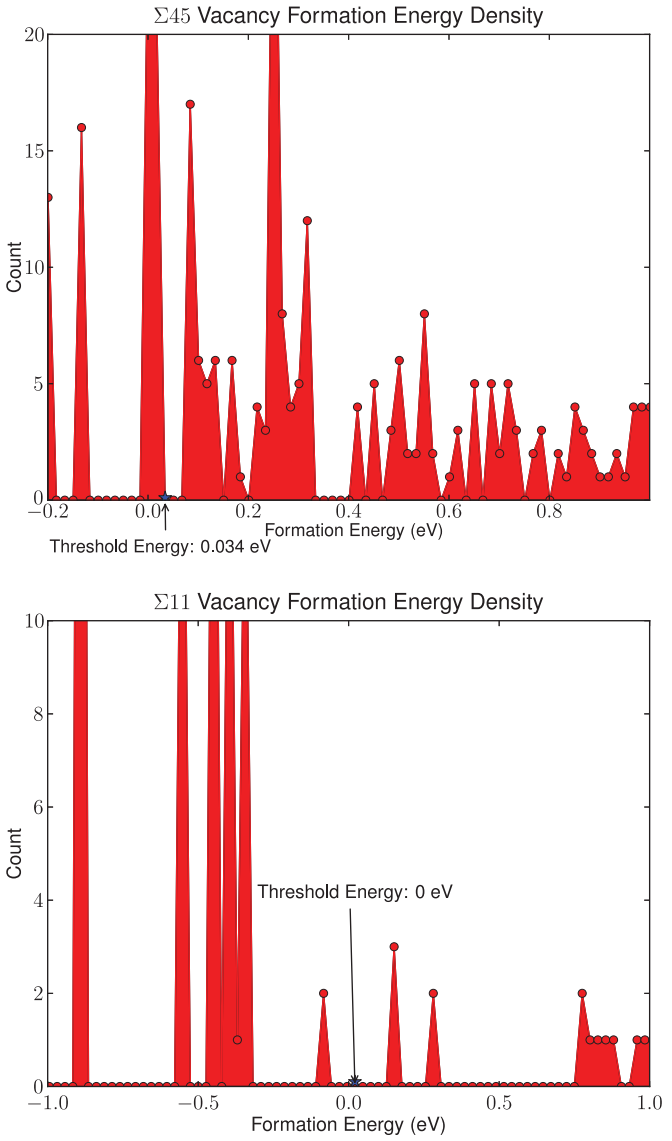

FIG. 2. (Color online) Vacancy formation energy densities for the Σ45 and symmetric Σ11 GBs. The points indicate the number of events involving a vacancy (either simple vacancy hops or recombination events) that had a final vacancy formation energy of the given value.

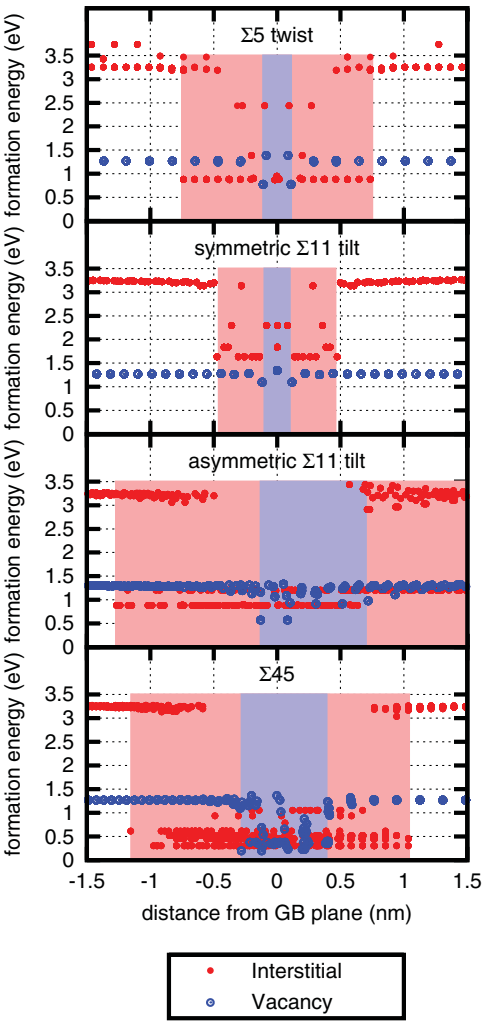

FIG. 3. (Color online) Interstitial and vacancy formation energies near each of the four grain boundaries considered in this study as a function of the initial distance of the defect from the grain boundary plane. The shaded regions indicate regions in which interstitials (light red) and vacancies (light blue) interact (energy is reduced by more than 10%) with boundary.

longer-ranged interactions with vacancies near those dislocations and is manifested in the set of lower-energy vacancy positions shown in Fig. 3 for distances greater than 0.2 nm. In general, we find that the GBs with symmetric character (Σ3, symmetric Σ11, and Σ5 twist) have narrower interaction widths than those with asymmetric character (asymmetric Σ11 and Σ45), indicating that the symmetry of the GB may determine this interaction distance. On the other hand, from Table II we see that, in general, the interaction strength of GBs with defects becomes stronger as the GB energy increases. The Σ3 twin and the Σ45 are two extreme examples of this trend. However, variations do exist, such as in the relative strengths of the Σ5 twist and asymmetric Σ11.

These results indicate that the interaction of defects with a given GB is very sensitive to the GB structure and energy, both in terms of how strongly the defect is absorbed into the GB (the decrease in formation energy at the GB) and how far from the GB the defect begins to interact with the GB. This implies that these GBs would have very different effects on radiation-induced defects. One might speculate, for example, that the Σ45 GB will have the greatest impact on radiation damage evolution, as it has both the strongest and longest interaction with defects. How a given GB modifies the behavior of radiation-induced defects manifests via two phenomena: changes in the number of defects produced in collision cascades and the subsequent evolution of those defects. In the next section, we investigate the first effect. The longer time evolution of defects will then be considered.

B. Damage production near boundaries

Using molecular dynamics (MD), we examine the modification in the number of defects surviving in the bulk after collision cascades on the picosecond time scale as a function of GB type and initial distance of the primary knock-on atom

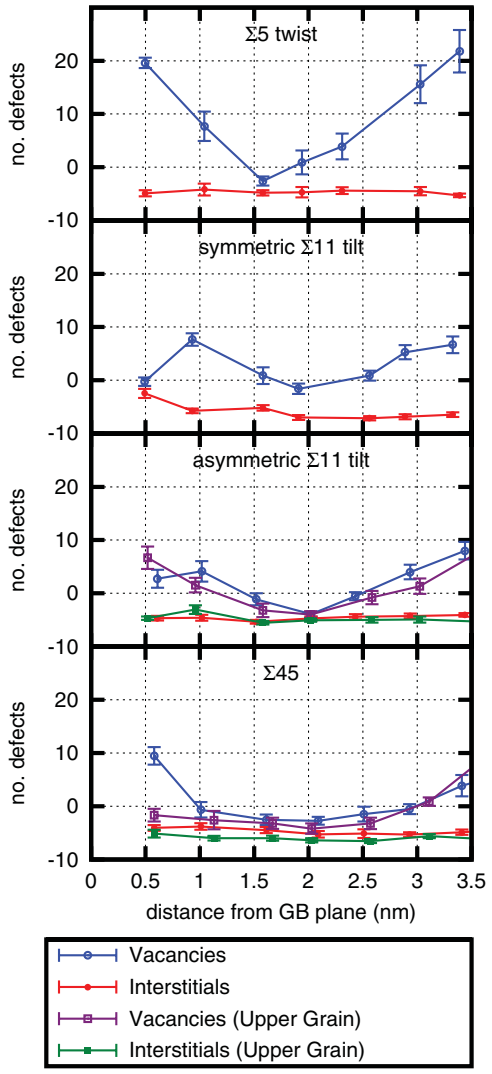

FIG. 4. (Color online) Number of interstitials and vacancies produced in the bulk region near each of the four grain boundaries considered in this study as a function of the initial distance of the PKA. Numbers are relative to the number of defects (Frenkel pairs) produced in equivalent cascades in single crystals. The statistics are based on 10–15 simulations at each PKA distance and the error bars represent the standard error. For the Σ5 twist and symmetric Σ11 tilt boundaries, only one set of values is given as the structure of the boundary is symmetric with respect to the grain boundary plane. For the other two boundaries (asymmetric Σ11 tilt and Σ45 asymmetric tilt), two sets of values for each type of defect are given, for the cascades initiated in the lower and upper grains (labeled explicitly).

(PKA) from the boundary plane. As detailed in Sec. II, all simulations were performed at 300 K with PKA energies of 4 keV, directed towards the grain boundary plane. We find that the Σ3 twin does not have any clear influence on defect production; damage production near this boundary is similar to that in a single crystal. This is not surprising as this GB interacts only very weakly with point defects: there is no thermodynamic driving force to trap defects. The results for the other four GBs are presented in Fig. 4; the results for the symmetric Σ11 GB were originally presented in Ref. 26. In Fig. 4, the number of defects are presented relative to the number of Frenkel pairs produced in the single crystal from cascades with the same PKA orientation. As with the defect interactions with the GB, there are aspects of the produced damage that are common to all four GBs, but there are again significant differences. Focusing on the common features, all four GBs exhibit strong absorption of interstitials for all distances considered. That is, the number of interstitials remaining in the bulk grain after the cascade is much smaller than the number produced in equivalent single-crystal cascades. Further, the number of vacancies produced typically follows a U-shaped curve for all four GBs, with more vacancies produced when the PKA is closer to or further from the grain-boundary plane than at intermediate distances. This shape has a simple physical explanation: the minimum in the defect production occurs when the cascade maximally overlaps with the GB plane and the vacancies are directly created in the GB. Overall, these four GBs exhibit biased absorption of interstitials over vacancies for the entire distance range considered.

However, examination of the number of surviving vacancies in the bulk region reveals that there are significant differences that can be attributed to the atomic structure of the GB. While the greatest number of excess vacancies are typically about 8–10 for most GBs, for the Σ5 twist, many more vacancies (a factor of 2 more) are produced. Inspection of the damage reveals that, near this GB, cascades produce a much larger number of large vacancy clusters, including stacking fault tetrahedra (SFTs), than for the other GBs. This indicates that the number of interstitials absorbed into the Σ5 twist GB is much greater than for the other GBs. This behavior was not anticipated based on the defect thermodynamics shown in Fig. 3 and summarized in Table II, which might have suggested that the twist GB should behave similarly to the symmetric Σ11. These differences can be attributed to the ability of the GB to absorb interstitials: an excess vacancy concentration only occurs because the GB, during the collision cascade, absorbs interstitials before they could recombine with vacancies. The Σ5 twist GB exhibits such a high number of produced vacancies because it absorbed a larger quantity of interstitials than the other GBs.

In addition, while the number of vacancies produced near all four GBs (including from both directions for the two asymmetric GBs) exhibits a minimum at PKA distances between 1.5 and 2 nm for our simulation conditions, the width of this minimum is very sensitive to the GB structure. For example, the range of PKA distances over which the two symmetric GBs result in vacancy numbers less than the single crystal (relative number of defects produced is less than zero) is relatively narrow, on the order of 0.5 nm, but is significantly larger (1–1.5 nm) for the two asymmetric GBs. This is especially true for the Σ45 GB, which shows vacancy-suppressed regions of 2 nm or more.

Figure 5 offers more insight into the processes by which the interstitials become absorbed into the GB during the damage event. In principle, there are two mechanisms by which the interstitials can be absorbed into the GB: directly during the collision cascade or via post-cascade diffusion to the boundary. Figure 5(a) shows the number of defects in the grain, defined as 6 Å or further away from the boundary, as a function of time. Even by a very short time of 10 ps,

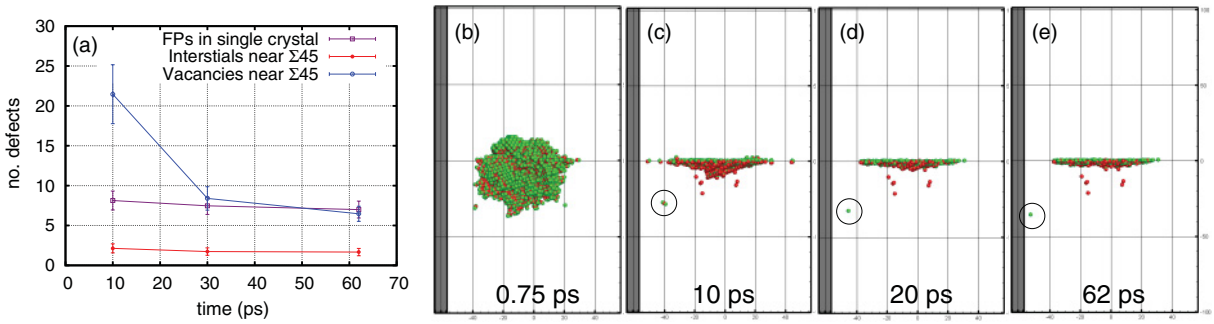

FIG. 5. (Color online) Details of collision cascades near the Σ45 GB. (a) The number of defects remaining in the grain away from the grain boundary as a function of time and in the single crystal. Points are averaged over 15 MD simulations and the error bars represent the standard error. (b)–(e) Snapshots of the defect structure near the grain boundary as the cascade settles and the GB reconstruction evolves. The green spheres represent interstitials, while red spheres are vacancies. In (c)–(e), one interstitial that is created in the grain interior is circled, highlighting that on these time scales it does not diffuse significantly.

the interstitial content, compared to the single crystal, is very small. This suggests that the vast majority of absorption occurs during the collision cascade. Further, if the primary driver of absorption were post-cascade diffusion, we would expect to see post-cascade vacancy numbers near the GBs more or less similar in magnitude to vacancy numbers in the single crystal. However, as shown in Fig. 4, the vacancy numbers near the GBs are very different from the corresponding single-crystal values. Moreover, on these time scales, we only expect modest evolution of interstitial content due to defect diffusion, and that is exactly what we see in Fig. 5(a). In fact, in Figs. 5(c)–5(e), there is an interstitial in the grain interior that only jumps a few times over the 50 ps shown, indicating that interstitial diffusion is not fast enough to account for all interstitials diffusing to the grain boundary on these time scales. The vacancy numbers do evolve significantly; this is a consequence of a complex reconstruction of the GB that anneals somewhat on the time scale simulated [see Figs. 5(b)–5(e)]. Clearly, this vacancy evolution is not a consequence of interstitial-vacancy annihilation as the interstitial content remains essentially constant over this time.

These results reveal significant differences in how different GBs modify damage production during cascades and thus imply very different behavior in terms of radiation tolerance of Cu with different GB distributions. If we limit our consideration to low temperatures, where thermal migration of defects can be neglected, the defect content within the material during irradiation will essentially be the integrated number of defects produced in individual cascades. This suggests that Cu with a large number of Σ5 twist GBs would experience a much higher damage accumulation rate than Cu samples containing more general GBs such as the Σ45 GB, which would maximally suppress defect production. Generically, however, GBs in Cu result in the production of more vacancies during cascades than if they were not present, thus enhancing radiation damage accumulation in the absence of thermally assisted events. Finally, all of these GBs strongly absorb interstitials, more so than vacancies, so in all cases the end result of the collision cascades is a GB loaded with interstitials with some number of vacancies residing in the nearby bulk.

C. Vacancy interaction with loaded boundaries

For most irradiation conditions of interest, temperatures are sufficiently high that point defects are mobile on relevant time scales. Thus, as shown in the previous section, while GBs in Cu result in more damage production during irradiation than if they were not present, thermally activated processes will be crucial for understanding damage evolution under most conditions. In our previous work,[26] we found that the interstitials loaded into the GB during the collision cascades could interact with the residual vacancies in the bulk over relatively long distances and short time scales via processes we termed "interstitial emission." Further, we determined that a signature of the propensity for these types of events to occur was revealed by the interaction of vacancies with the interstitial-loaded GBs. Here, we examine vacancy interaction with loaded versions of the four non-twin GBs to determine how the atomic structure of the GB influences the interstitial emission effect. Loading effects have not been examined for the Σ3 twin as it does not exhibit any significant interactions with interstitials.

However, before discussing the results, a few words on the interstitial emission process are warranted. In Ref. 26, we showed how interstitials can annihilate vacancies via processes in which the interstitial "emits" from the GB with relatively low barriers. These emissions only occur when the vacancies are nearby and available for recombination. The annihilation of the two defects releases a large amount of energy and is the driving force for the process. The binding energies (or segregation energies) of interstitials at the GBs are very large, as illustrated in Fig. 3, and the associated time scales for interstitials to emit into the grain from the GB without recombining with vacancies would be extremely large. We used the term "interstitial emission" to describe this annihilation process since, as revealed by nudged elastic band calculations, the collective motion of the atoms begins with the interstitials at the GB, not with the atoms neighboring the vacancy.

Figure 6 shows the formation energy of a vacancy near each of the four GBs loaded with 10 interstitials, used to mimic the post-cascade damaged structures. In each case, the vacancy formation energy is strongly modified by the

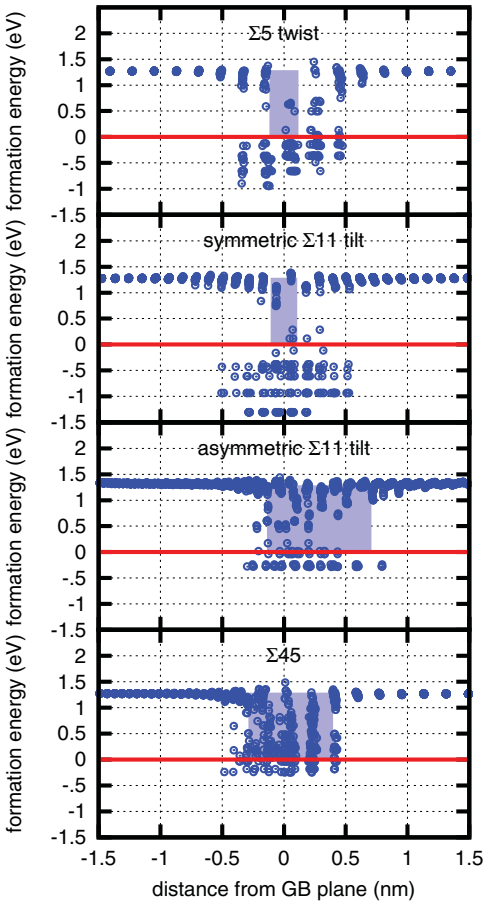

FIG. 6. (Color online) Vacancy formation energy near each of the four grain boundaries considered in this study, loaded with 10 interstitials, as a function of the initial position of the vacancy. The shaded regions indicate zones in which the vacancy formation energy was modified by the pristine boundary, as shown in Fig. 3 for comparison.

interstitials loaded into the GB. The width of the interaction zone increases appreciably, at least by 0.5 nm in most cases. Further, unstable vacancy sites appear, as indicated by the sites with negative formation energy. Vacancies placed at these sites spontaneously recombine with interstitials loaded into the GB via interstitial emission processes. This happens for all four GBs.

Again, there are quantitative differences in how vacancies interact with the loaded GBs, depending on the structure. First, the effects of loading are strongest for the symmetric GBs, with the relative increase in the interaction zone and the strength of interaction (the relative change in formation energies) much greater than for the asymmetric GBs. This is a consequence of two factors. First, the asymmetric GBs, in their pristine form, already had significantly stronger interactions with vacancies than the symmetric GBs. Thus, the relative effects are stronger on the symmetric GBs than the asymmetric ones. Second, interstitial formation energies are low in the pristine asymmetric GBs. Thus, when interstitials are loaded into the GB, they are more easily accommodated than in the symmetric GBs. When an interstitial annihilates with a vacancy near the loaded symmetric GBs, because they are relatively high in energy, more energy is gained through the annihilation process. This is more easily seen if one considers the case of a hypothetical GB in which interstitial formation energies are zero. Vacancies annihilating these interstitials can at most release the bulk formation energy of vacancies (1.27 eV) as there is no interstitial formation energy to recover. In that case, all vacancy formation energies with such a GB loaded with interstitials would be zero or greater, never negative. This also indicates that negative formation energies for vacancies, as reported in Fig. 6, are a sufficient but not necessary indicator of spontaneous interstitial emission processes. Spontaneous interstitial emission processes can occur at sites where the vacancy formation energy near the loaded GB is positive, as discussed in Sec. II.

D. Spontaneous versus thermally activated recombination

The analysis presented in Fig. 6 shows the interaction between interstitials loaded into the GBs and the residual vacancies. However, at finite temperature, more processes are possible by which interstitials, with some finite barrier, can recombine with those vacancies than at $T = 0$ K. As detailed in Sec. II, we have used a saddle-point searching algorithm to find all of the possible single-barrier vacancy-interstitial recombination processes near each of the GBs loaded with 10 interstitials. In Fig. 7, the lowest barrier process for each site is reported. That is, of the possible events for a vacancy at each site, the lowest barrier event that leads to recombination with interstitials at the GB is shown. To better understand the observed behavior, the structure of the interstitial-loaded GB, as found by the reference lattice method (see Sec. II), is shown in the inset of each panel of the figure.

In all four cases, the range of the interaction between the loaded GB and the residual vacancies increases as finite-barrier processes are considered, typically by 1–2 atomic planes from the GB, compared to spontaneous recombination. Typically, the processes are grouped into three shells around the core of the loaded interstitials: an inner shell where recombination is spontaneous, an intermediate shell where finite but small barrier recombinations occur ($0 < E_a < \frac{1}{2}E^m_{\rm vac}$, where $E^m_{\rm vac}$ is the bulk migration barrier for the Cu vacancy, about 0.7 eV), and an outer shell of higher barrier processes ($\frac{1}{2}E^m_{\rm vac} < E_a < E^m_{\rm vac}$). Thus, the differences in how each of the loaded GBs interact over longer distances with the residual vacancies are primarily a consequence of how the interstitials are accommodated into the GBs in the first place. As shown in the insets, the loaded structures are significantly different. In the case of the two Σ11 GBs, the loaded interstitials form a compact structure, aligning in clusters along the tilt axis of the GB. In contrast, for the Σ5 twist GB, this clustering is not as pronounced. In this case, the loaded interstitials are not confined to one plane at the GB, but rather occupy up to three different atomic planes. This might explain the behavior observed in Fig. 4 in which the Σ5 twist GB absorbs more interstitials than the other GBs: the GB is able to accommodate interstitials not only on the plane of symmetry, but nearby as well.

There are other aspects of the vacancy-interstitial recombination behavior that are related to the GB structure. For example, the asymmetric natures of the asymmetric Σ11 tilt and the Σ45 GBs manifest themselves in the

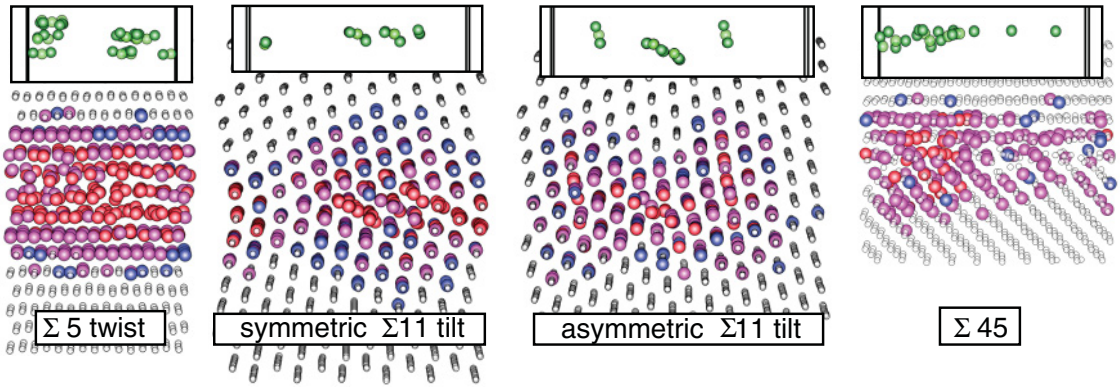

FIG. 7. (Color online) Barriers for vacancy-interstitial recombination at the Σ5 twist, symmetric Σ11 tilt, asymmetric Σ11 tilt, and Σ45 tilt + twist grain boundaries, each loaded with 10 interstitials. The coloring scheme for each of the main figures is as follows: red spheres indicate sites where vacancies spontaneously recombine with interstitials at the boundary, purple spheres are sites where the recombination barrier E_a is $0 < E_a < \frac{1}{2}E^m_{\text{vac}}$, and blue spheres are sites where $\frac{1}{2}E^m_{\text{vac}} < E_a < E^m_{\text{vac}}$, where E^m_{vac} is the migration barrier for vacancies in bulk Cu. Small white spheres are sites for which there are no single-barrier recombination events below E^m_{vac}. The structure of the loaded boundaries is shown in the insets in which dark green spheres indicate interstitials and light green spheres indicate vacancies relative to the pristine structure.

vacancy-interstitial interaction. In the case of the asymmetric Σ11 GB, the presence of Schockley partials in the upper grain is reflected both in the structure of the loaded interstitials (the two interstitial clusters with orientation perpendicular to the grain boundary plane) and the interaction with vacancies. The interstitial-vacancy interaction extends further along those partials than it does in other regions of the GB. In the case of the Σ45 GB, the interaction between interstitials and vacancies extends much further into the lower grain than the upper grain. Clearly, the behavior of the vacancy-interstitial interaction is directly related to the structure of the loading at the interface. Thus, it is how different GBs accommodate interstitials that governs the propensity for mechanisms such as interstitial emission.

Table II quantifies the behavior shown in Fig. 7. The two symmetric GBs, Σ5 twist and symmetric Σ11 tilt, show the greatest influence from these finite-barrier recombination processes. In both cases, the recombination width, typically defined by those sites at which the formation energy of vacancies is negative and not to be confused with the interaction width defined previously, nearly doubles for both of these GBs when considering finite-barrier recombination compared to spontaneous recombination. For the asymmetric GBs, the effect is not as strong. Further, there is also a correlation between the structure of the GB and the number of sites at which spontaneous recombination can occur. This is again greatest for the two symmetric GBs. However, there is not as clear a trend between GB structure and the number of sites for which finite-barrier recombination occurs, although this might be at least partially related to differences in the sizes of boundary unit cells used for the different GB structures.

As a consequence of interstitial loading, symmetric GBs become less stable than asymmetric GBs, due to the high cost of putting interstitials in those GBs. Thus, interstitial emission processes, while occurring at all four GBs, are most prevalent at the symmetric GBs. This has consequences for the evolution of the material under irradiation. At intermediate temperatures, where vacancy diffusion is still suppressed and vacancies can not directly diffuse to GBs, the interstitial emission mechanism is one mechanism that can still occur, leading to interstitial-vacancy recombination. For Cu with a hypothetical microstructure filled with symmetric GBs such as Σ5 twist and Σ11, interstitial emission effects should be stronger than if asymmetric GBs were present. However, as described above, asymmetric GBs lead to fewer produced defects in the first place, so the overall consequence may be similar. How these two effects, loading and unloading, interplay to determine the radiation tolerance of the material as a function of temperature is an open question.

IV. DISCUSSION AND CONCLUSIONS

We have examined the role that the atomic structure of GBs has on the interaction of those GBs with defects in Cu, focusing on five GB structures that vary in their properties. Except for the Σ3 coherent twin GB which interacts very weakly with defects, we find that there are features common to how defects interact with all of these GBs: relatively strong interaction of defects with the pristine structure, biased absorption of interstitials over vacancies during collision cascades, and enhanced reactivity of vacancies near GBs loaded with interstitials. However, we also find that there are significant differences in how strongly these phenomena manifest themselves in the presence of different GB structures.

The conclusions from our modeling work are consistent with experimental observations in the literature.[6–8,31] Seigel *et al.*[6] measured the width of the SFT denuded zone near a number of GBs in quenched polycrystalline gold to determine the vacancy sink strength of those GBs; a wider denuded zone indicates a stronger sink for vacancies. They found that the Σ3 coherent twin is a poor sink. In contrast, while the vacancy sink strength is stronger and similar in magnitude for other types of GBs, variations in the denuded zone width were observed, although, as pointed out by the authors, the differences could be within the uncertainties of the measurement. Similar observations and conclusions are also found in the work of Basu and Elbaum on aluminum.[31] Thorsen *et al.*[7] investigated helium bubble sizes and bubble denuded zone widths near

many types of GBs in copper. They showed that the Σ3 coherent twin does not assist helium precipitation, consistent with the work of Barnes *et al*.[8] In addition, they found that although the bubble denuded zone width is not sensitive to the GB type, the size of helium bubbles at the GBs does depend on GB structure: the bubble size increased with the GB energy. This observation is consistent with our results shown in Table II that the boundary-defect interaction strength tends to increase with the increasing GB energy.

The primary consequence of loading GBs with interstitials is that the strength of interaction with vacancies increases significantly. Here, we only put 10 interstitials at each GB, a defect concentration that is far from saturation. We expect that the loading effects would be even stronger as the concentration of defects at the GBs increases. In terms of rate theory models of radiation damage, this would imply that sink strength is not a static quantity but varies as GBs absorb radiation-induced defects, fluctuating as the defect content at the GB changes. For nanocrystalline material,[10] where the density of GBs is extremely large, this phenomenon may be important.

Thus, while all of these GBs would generically influence radiation damage in a similar manner, detailed predictions of long-time evolution of the material would require knowledge of the specific GBs present in the microstructure. This would be especially true for low-temperature irradiations. For Cu, such low temperatures are primarily of academic interest, but for other materials, such as tungsten or oxide ceramics, the relevant temperatures would be much higher. Further, we expect that the behavior described here is relatively common beyond just fcc materials. For example, we have found similar thermodynamics of defects at GBs as well as biased absorption of interstitials at GBs in TiO_2.[32,33] Caution is warranted in extending these results to other systems. For example, the Σ3 coherent twin in Cu essentially has no interaction with defects. However, in complex oxides such as $SrTiO_3$,[34] Σ3 coherent twins can interact very strongly with defects. In such cases, we speculate that they will behave similarly to other types of GBs in that material. Further, these effects have not been observed in simulations of SiC.[11]

To conclude, as long as GBs are reasonably strong sinks for defects, they behave qualitatively similarly in terms of how they modify radiation damage. However, the specific GB structure has a significant role in the radiation tolerance. The magnitude of the biased absorption of interstitials over vacancies is very sensitive to GB structure. Further, the propensity of interstitial emission also depends on the GB structure. Therefore, the effective defect production rate during irradiation, as modified by the GBs, and the GB sink strength, as determined by the concentration of interstitials at each GB, thus depend on the types and distributions of GBs in the material.

ACKNOWLEDGMENTS

The authors are grateful to A. P. Sutton for helpful discussions. This material is based upon work supported as part of the Center for Materials at Irradiation and Mechanical Extremes, an Energy Frontier Research Center funded by the US Department of Energy (US DOE), Office of Science, Office of Basic Energy Sciences (OBES) under Award No. 2008LANL1026. A.F.V. was supported by the US DOE OBES, Materials Sciences and Engineering Division. The cascade simulations near the Σ45 GB performed by X.M.B. were conducted and analyzed under his present employment in the Center for Materials Science of Nuclear Fuel (CMSNF) at Idaho National Laboratory, an Energy Frontier Research Center funded by the US Department of Energy, Office of Science, Office of Basic Energy Sciences under Award No. FWP 1356.

[1] F. Gao, H. L. Heinisch, and R. J. Kurtz, J. Nucl. Mater. **367–370**, 446 (2007).
[2] H. L. Tuller, Solid State Ionics **131**, 143 (2000).
[3] J. Nowotny, T. Bak, T. Burg, M. K. Nowotny, and L. R. Sheppard, J. Phys. Chem. C **111**, 9769 (2007).
[4] J. Wang, A. Misra, and J. P. Hirth, Phys. Rev. B **83**, 064106 (2011).
[5] J. Wang and A. Misra, Curr. Opin. Solid State Mater. Sci. **15**, 20 (2011).
[6] R. W. Siegen, S. M. Chang, and R. W. Balluffi, Acta Metall. **28**, 249 (1980).
[7] P. A. Thorsen, J. B. Bilde-Sorensen, and B. N. Singh, Scr. Mater. **51**, 557 (2004).
[8] R. S. Barnes, G. B. Redding, and A. H. Cottrell, Philos. Mag. **3**, 97 (1958).
[9] R. Yamada, S. J. Zinkle, and G. P. Pells, J. Nucl. Mater. **191–194**, 640 (1992).
[10] Y. Chimi, A. Iwase, N. Ishikawa, M. Kobiyama, T. Inami, and S. Okuda, J. Nucl. Mater. **297**, 355 (2001).
[11] N. Swaminathan, P. J. Kamenski, D. Morgan, and I. Szlufarska, Acta Mater. **58**, 2843 (2010).
[12] T. D. Shen, S. Feng, M. Tang, J. A. Valdez, Y. Q. Wang, and K. E. Sickafus, Appl. Phys. Lett. **90**, 263115 (2007).
[13] A. Misra, M. J. Demkowicz, X. Zhang, and R. G. Hoagland, JOM **59**, 62 (2007).
[14] H. A. Atwater and W. L. Brown, Appl. Phys. Lett. **56**, 30 (1990).
[15] C. Herzig, Y. Mishin, and S. Divinski, Metall. Mater. Trans. A **33**, 765 (2002).
[16] S. Watanabe, Y. Takamatsu, N. Sakaguchi, and H. Takahashi, J. Nucl. Mater. **283–287**, 152 (2000).
[17] M. R. Sorensen, Y. Mishin, and A. F. Voter, Phys. Rev. B **62**, 3658 (2000).
[18] A. Suzuki and Y. Mishin, Interface Sci. **11**, 131 (2003).
[19] M. A. Tschopp, M. F. Horstemeyer, F. Gao, X. Sun, and M. Khaleel, Scr. Mater. **64**, 908 (2011).
[20] H. S. Lee, T. Mizoguchi, J. Mitsui, T. Yamamoto, S. J. L. Kang, and Y. Ikuhara, Phys. Rev. B **83**, 104110 (2011).
[21] R. J. Kurtz and H. L. Heinisch, J. Nucl. Mater. **329–333**, 1199 (2004).
[22] A. Suzuki and Y. Mishin, Interface Sci. **11**, 425 (2003).
[23] F. J. Pérez-Pérez and R. Smith, Nucl. Instrum. Methods Res. Sect. B **164–165**, 487 (2000).

[24]M. Samaras, P. M. Derlet, H. Van Swygenhoven, and M. Victoria, Philos. Mag. **83**, 3599 (2003).
[25]M. Samaras, P. M. Derlet, H. Van Swygenhoven, and M. Victoria, Phys. Rev. Lett. **88**, 125505 (2002).
[26]X. M. Bai, A. F. Voter, R. G. Hoagland, M. Nastasi, and B. P. Uberuaga, Science **327**, 1631 (2010).
[27]Y. Mishin, M. J. Mehl, D. A. Papaconstantopoulos, A. F. Voter, and J. D. Kress, Phys. Rev. B **63**, 224106 (2001).
[28]C. Jiang, S. A. Maloy, and S. G. Srinivasan, Scr. Mater. **58**, 739 (2008).
[29]L. J. Vernon, Ph.D. thesis, Loughborough University, 2010.
[30]M. J. Demkowicz, O. Anderoglu, X. Zhang, and A. Misra, J. Mater. Res. **26**, 1 (2011).
[31]B. K. Basu and C. Elbaum, Acta Metall. **13**, 1117 (1965).
[32]B. P. Uberuaga and X. M. Bai, J. Phys.: Condens. Matter **23**, 435004 (2011).
[33]X. M. Bai and B. P. Uberuaga, Philos. Mag. **92**, 1469 (2012).
[34]B. P. Uberuaga, S. Choudhury, X. M. Bai, and N. A. Benedek, Scr. Mater. **66**, 105 (2011).